

# Joint Learning of Generative Translator and Classifier for Visually Similar Classes

ByungIn Yoo<sup>1,2</sup>, Tristan Sylvain<sup>3</sup>, Yoshua Bengio<sup>3</sup>, Junmo Kim<sup>1</sup>

<sup>1</sup>Korea Advanced Institute of Science and Technology

<sup>2</sup>Samsung Advanced Institute of Technology

<sup>3</sup>Montreal Institute for Learning Algorithms

byungin.yoo@kaist.ac.kr, tristan.sylvain@gmail.com, yoshua.bengio@mila.quebec, junmo.kim@kaist.ac.kr

## Abstract

In this paper, we propose a Generative Translation Classification Network (GTCN) for improving visual classification accuracy in settings where classes are visually similar and data is scarce. For this purpose, we propose joint learning to train a classifier and a generative stochastic translation network end-to-end. The translation network is used to perform on-line data augmentation across classes, whereas previous works have mostly involved domain adaptation. To help the model further benefit from this data-augmentation, we introduce an adaptive fade-in loss and a quadruplet loss. We perform experiments on multiple datasets to demonstrate the proposed method's performance in varied settings. Of particular interest, training on 40% of the dataset is enough for our model to surpass the performance of baselines trained on the full dataset. When our architecture is trained on the full dataset, we achieve comparable performance with state-of-the-art methods despite using a light-weight architecture.

## Introduction

Generative models have received significant interest in the past years. Although recent models can generate realistic and diverse data, more study is needed to ascertain whether the methods can be useful in enhancing classification accuracy on hard condition such as visually similar classes or lack of data. For example, face liveness detection in biometrics is a crucial problem where it is hard to distinguish between real faces and printed fake faces, because examples from the two classes are very similar (Akbulut et al.2017; Atoum et al.2017; Tang et al.2018; Song, Zhao, and Lin2018; Li et al.2018; Liu, Jourabloo, and Liu2018). In this application, obtaining a high true acceptance ratio (TAR) and a low false acceptance ratio (FAR) is important as a high TAR is essential for user convenience, whereas a low FAR results in better security. This paper is motivated by two questions:

- If two classes,  $A$  and  $B$ , are visually very similar, how can we improve classifiers by employing cross-class generative models?

The research of this paper was conducted from March 2018 to February 2019.

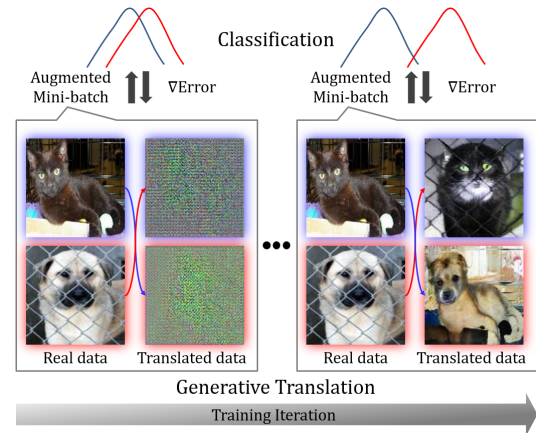


Figure 1: A generative translation model progressively generates samples to augment data in mini-batch for joint training of a classifier.

- When data is scarce, how can we use generative models to learn better representations?

In practice, most past approaches to solving these two questions fall in two categories. The first one is using complex models, which are often hard to train, and make it difficult to perform fast inference in settings with limited computing resources, such as on a smartphone. The second is to collect large amounts of training data, which is costly, time-consuming, and not always straightforward. In this paper, we propose a Generative Translation Classification Network that uses the translation model of visual classes to assist the training of the classifier via exploiting joint learning. If the translation model is able to effectively augment the quantity of training samples we expect both the issue of having closely distributed classes, and the lack of sufficient amounts of training data to be mitigated. We should note the similarity of our proposed method with the way the brain learns. There is biological evidence that long-term memory is formed by the collaboration between the hippocampus and the prefrontal cortex (Preston and Eichenbaum2013). The hippocampus recalls slightly distorted memories, in a way which inspired our translation network generating variations on training ex-

amples. The prefrontal cortex uses such memories, and has a role analogous to the classifier we used. In summary, our contributions are the following:

- To augment mini-batch data (AMB) during training, we use inter-class translated samples based on joint learning of a translation model and a classifier. Specifically, half the training samples seen by the classifier are inter-class translated samples that are stochastically generated (ST), while the other half of the samples are real samples of training data to preserve data distribution. This is a novel attempt to couple a generative translation network and a classifier in a unified architecture for improving classification of visually similar classes.
- Early on during joint learning, translated samples are of poor quality. We use adaptive fade-in training (AF) for the classifier, automatically adjusting the importance of real and translated samples to gradually adapt the influence from translated samples. We design a novel quadruplet loss (QL) that helps preserve intra-class distribution and taking inter-class distribution apart, even though generated samples are used for training. This is due to the fact that this loss encourages similarity between the embeddings of real and intra-class translated images, and dissimilarity between the embeddings of inter-class samples.

## Related work

Since the introduction of generative adversarial networks (GANs) (Goodfellow et al.2014), many GAN-based generative models have been introduced, e.g. (Mirza and Osindero2014; Chen et al.2016; Odena, Olah, and Shlens2016; Antoniou, Storkey, and Edwards2017; Creswell et al.2018). A typical issue is mode collapse, reduced diversity of generated samples, which would be detrimental to improve classification accuracy in our setup. In addition to this, our specific need for inter-class generated samples is difficult to meet with classical GANs, hence we focus on adversarial translation models. Domain translation has received renewed interest in recent years, thanks in large part to the use of adversarial methods. The first results using adversarial training used paired samples (Isola et al.2017). More recent developments using cycle consistency allow for unsupervised domain translation using unpaired samples (Taigman, Polyak, and Wolf2016;Zhu et al.2017a;Liu, Breuel, and Kautz2017). Finally, newer methods extend this approach to problems requiring many-to-many mappings or multi-modal data distributions (Choi et al.2017;Zhu et al.2017b; Huang et al.2018;Almahairi et al.2018;Lee et al.2018). The power of these approaches lies in being able to learn such transformations without requiring examples of a one-to-one mapping between training data in source and target domains.

Multiple works have used the discriminators of GANs as semi-supervised learning classifiers (Springenberg2015; Dumoulin et al.2016; Gan et al.2017; Chongxuan et al.2017; Dai et al.2017). Typically, the semi-supervised classifiers take a tiny portion of labeled data and a much larger amount of unlabeled data from the same domain. The goal is to use both labeled and unlabeled data to train a neural network so that it can map a new data point to its correct class (Odena2016).

A simple yet effective idea for semi-supervised learning is to turn a classification problem with  $n$  classes into a classification problem with  $n + 1$  classes, with the additional class corresponding to fake images (Salimans et al.2016). However, the methods are not directly augmenting data of existing classes, since they assume generated data is a new class.

In terms of cost functions, the feature matching loss (Salimans et al.2016) is addressed to prevent instability of GANs from overtraining on the discriminator. Specifically, the generator is trained to match the expected value of the features on an intermediate layer of the discriminator. While feature matching losses bring benefits, a cost function that can account for inter- and intra-class relationships is required in our case. Deep learning networks with variants of a triplet loss become common methods for face verification (Schroff, Kalenichenko, and Philbin2015) and person re-identification (Chen et al.2017). In spite of the trends, applying on the generative models are rarely considered.

From another perspective, between-class data augmentation methods have been proposed (Tokozume, Ushiku, and Harada2018). Images are generated by mixing two training images belonging to different classes with a random ratio. The training procedure seeks to minimize the KL-divergence between the outputs of a trained model, and a target computed by interpolating the two one-hot target vectors of the initial examples using the same ratio. Even though the methods achieve superior results on visual recognition, it is not clear whether the classifier learns shaper and more diverse data on visually similar classes.

In this paper, we are using generated translation images to augment data in each mini-batch and training of a classifier. Even though many previous methods have tackled generative models, this work focuses on joint learning that improve classification accuracy for visually similar images.

## Proposed methods

We design a unified deep network architecture that combines a classifier  $C$  and a generative translation model  $G$  to perform on-line data augmentation of the mini-batch. The proposed architecture is explained in Figure 2.

### Formulation of proposed methods

Let  $\{x_y^i : 1 \leq i \leq n, y \in Y\}$  be a dataset such that  $x_y^i \in X$  is the  $i$ -th sample belonging to class  $y \in Y$ . We consider a learning algorithm that trains a classifier

$$C : X \rightarrow Y \quad (1)$$

by jointly using a generative translation model  $G(\tilde{x}|x)$ . Our goal is to improve the classifier  $C$  by utilizing the on-line translated samples  $\tilde{x}$  as additional training data.

More formally,  $C$  is a classifier to discriminate two-class cases, where  $Y = \{A, B\}$ . Generative translation models  $G$  are employed to produce  $\tilde{x}$  from  $x$  as:

$$\tilde{x}_A^i = G_{BA}(x_B^i, z_{BA}), \quad (2)$$

$$\tilde{x}_B^i = G_{AB}(x_A^i, z_{AB}), \quad (3)$$

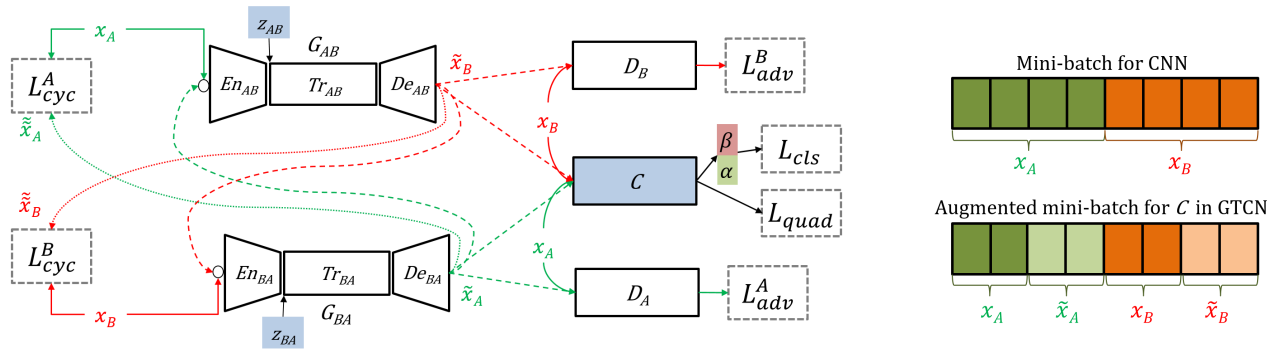


Figure 2: Overview of the proposed Generative Translation Classification Network : (Left)  $G_{AB}$  is a translator from class  $A$  to  $B$ , while  $G_{BA}$  is a corresponding translator from class  $B$  to  $A$ .  $G_{AB}$  consists of three main blocks, an encoder  $En_{AB}$  (three convolutional layers), transformer  $Tr_{AB}$  (nine residual blocks), and decoder  $De_{AB}$  (two deconvolutional layers and one convolutional layer). Likewise,  $G_{BA}$  consists of  $En_{BA}$ ,  $Tr_{BA}$ , and  $De_{BA}$ . Random noise  $\{z_{AB}, z_{BA}\} \in \mathbb{R}^{32 \times 32 \times 3}$  for stochastic translation is sampled from a uniform distribution over  $[-1, 1]$  and concatenated to the output maps of  $En_{AB}$  and  $En_{BA}$ .  $D_A$  and  $D_B$  are the corresponding discriminators of adversarial training for classes  $A$  and  $B$  respectively.  $C$  is a simple classifier consisting of six convolutional layers over classes  $A$  and  $B$ .  $\alpha$  and  $\beta$  are the trainable parameters of the adaptive fade-in loss.  $x_A$  and  $x_B$  are real samples from classes  $A$  and  $B$  respectively. The corresponding translated samples are denoted by  $\tilde{x}_B$  and  $\tilde{x}_A$ . The cyclic reconstructed samples are  $\tilde{\tilde{x}}_A = G_{BA}(\tilde{x}_B)$  and  $\tilde{\tilde{x}}_B = G_{AB}(\tilde{x}_A)$ . Note that only  $C$  is used at test-time. Details of loss functions  $L^*$  are in proposed methods section. (Right) Comparison of mini-batch structure. A mini-batch used for training  $C$  in GTCN contains real and translated samples, while the baseline CNNs are only trained on real samples.

where  $x_A^i$  and  $x_B^i$  are real samples of class  $A$  and  $B$ ,  $z_{BA}$  and  $z_{AB}$  are tensors of random noise used for stochastic translation, and  $\tilde{x}_A^i$  and  $\tilde{x}_B^i$  are translated samples across the classes. One of our important contributions is to add a translator into the full pipeline for a classifier and to jointly train the translator and the classifier. Namely,  $G_{AB}$  and  $G_{BA}$  provide diverse and challenging data continuously for training classifier  $C$ . So, we suppose  $G_{AB}$  and  $G_{BA}$  generate effective images from the standpoint of decision boundary of the classifier.

**Definition of augmented mini-batch** The augmented mini-batch that is input to the classifier  $C$  during training is defined as follows:

$$AMB_k = \{x_A^i\}_{i=1}^m \cup \{\tilde{x}_A^i\}_{i=1}^m \cup \{x_B^i\}_{i=1}^m \cup \{\tilde{x}_B^i\}_{i=1}^m, \quad (4)$$

where  $k$  is the training iteration,  $m$  is the number of samples in each set. The  $\tilde{x}$ 's in  $AMB_k$  increase diversity of training data, while  $x$ 's preserve original distribution of training data.

**Loss of stochastic translator** Visual translation objective across classes is that a source class borrow underlying structure from a target class, while maintain style of the source class. To meet the needs, cycle consistency losses,  $L_{cyc}^A$  and  $L_{cyc}^B$ , are used to train stochastic translators,  $G_{AB}$  and  $G_{BA}$ . The objective is expressed as:

$$L_{cyc}^A = \mathbb{E}_{x_A \sim P_{data}} [\|G_{BA}(\tilde{x}_B, z_{BA}) - x_A\|_1], \quad (5)$$

$$L_{cyc}^B = \mathbb{E}_{x_B \sim P_{data}} [\|G_{AB}(\tilde{x}_A, z_{AB}) - x_B\|_1]. \quad (6)$$

For generating realistic images, an adversarial loss  $L_{adv}^A$  is applied to train  $D_A$  and  $G_{BA}$ . Similarly, an adversarial loss  $L_{adv}^B$  is applied to train  $D_B$  and  $G_{AB}$ . The objective is expressed as:

$$L_{adv}^A = \mathbb{E}_{x_A \sim P_{data}} [\log(D_A(x_A))] + \mathbb{E}_{x_B \sim P_{data}} [\log(1 - D_A(G_{BA}(x_B, z_{BA})))] , \quad (7)$$

$$L_{adv}^B = \mathbb{E}_{x_B \sim P_{data}} [\log(D_B(x_B))] + \mathbb{E}_{x_A \sim P_{data}} [\log(1 - D_B(G_{AB}(x_A, z_{AB})))] . \quad (8)$$

**Adaptive fade-in learning** In the early stages, translated samples in  $AMB_k$  are relatively poor and relying on them too much could be detrimental for training classifier  $C$ . We therefore design an adaptive fade-in loss (AF) that adapts the importance given to real and translated samples during training. The objective is defined as:

$$L_{cls} = \alpha \cdot \mathbb{E}_{x_A \sim P_{data}} [-\log(P(y=A|x_A))] + (1 - \alpha) \cdot \mathbb{E}_{x_B \sim P_{data}} [-\log(P(y=A|G_{BA}(x_B, z_{BA})))] + \beta \cdot \mathbb{E}_{x_B \sim P_{data}} [-\log(P(y=B|x_B))] + (1 - \beta) \cdot \mathbb{E}_{x_A \sim P_{data}} [-\log(P(y=B|G_{AB}(x_A, z_{AB})))] , \quad (9)$$

where  $\alpha$  and  $\beta$  are parameters between 0 to 1. We use a categorical cross-entropy loss  $L_{cls}$  on the Softmax output of  $C$ . The classification loss  $L_{cls}$  is used to train  $C$ ,  $G_{AB}$ , and  $G_{BA}$  by backpropagation. In the equation 9, the parameters  $\alpha$  and  $\beta$  control the relative importance of four training inputs,  $x_A$ ,  $\tilde{x}_A = G_{BA}(x_B, z_{BA})$ ,  $x_B$ , and  $\tilde{x}_B = G_{AB}(x_A, z_{AB})$  in  $AMB_k$ . Specifically,  $\alpha$  controls the relative weight given to real data  $x_A$  and augmented data  $\tilde{x}_A$  to train a classifier  $C$ . Similarly,  $\beta$  controls the relative importance given to real data  $x_B$  and augmented data  $\tilde{x}_B$  to train the classifier  $C$ .

**Quadruplet loss for inter/intra-class** We design a quadruplet loss for the proposed architecture that enforces explicit relationships between classes. The objective is defined as:

$$L_{quad} = \begin{aligned} & [\|f_C(x_A) - f_C(\tilde{x}_A)\|_2^2 - \|f_C(x_A) - f_C(\tilde{x}_B)\|_2^2 + \eta_a]_+ \\ & + [\|f_C(x_B) - f_C(\tilde{x}_B)\|_2^2 - \|f_C(x_B) - f_C(\tilde{x}_A)\|_2^2 + \eta_b]_+ \\ & + [-\|f_C(x_A) - f_C(x_B)\|_2^2 - \|f_C(\tilde{x}_A) - f_C(\tilde{x}_B)\|_2^2 + \eta_c]_+ , \end{aligned} \quad (10)$$

where  $[\cdot]_+ = \max(\cdot, 0)$ , and  $f_C(\cdot)$  denotes the embedding features of  $x_A, \tilde{x}_A, x_B$ , and  $\tilde{x}_B$  in  $AMB_k$  at the last feature layer of the classifier  $C$ . The thresholds  $\eta_a, \eta_b$ , and  $\eta_c$  are margins that are enforced between positive and negative pairs. Likewise  $L_{cls}, L_{quad}$  is used to train  $C, G_{AB}$ , and  $G_{BA}$ . The quadruplet loss encourages the similarity of intra-class samples and the dissimilarity of inter-class samples, which is useful for classification. Specifically, the intention of the designing the quadruplet loss considers all six pairs out of the four elements,  $x_A, x_B, \tilde{x}_A$ , and  $\tilde{x}_B$ . The first and second items in equation 10 are aim to minimize intra-class variation and maximizing means of inter-classes. The final term acts differently, it aims to auxiliary regulate the inter-class means.

**Overall training objective** The training objective of a classifier  $C$  in GTCN is:

$$L_C = L_{cls} + L_{quad}. \quad (11)$$

The training objective of translator  $G$  in GTCN is:

$$L_G = L_C + L_{adv}^A + L_{adv}^B + \lambda \cdot (L_{cyc}^A + L_{cyc}^B), \quad (12)$$

where  $\lambda$  is a weight parameter to adjust the relative importance of the cyclic consistency losses. Finally, we aim to optimize:

$$G_{AB}^*, G_{BA}^* = \arg \min_{\{G_{AB}, G_{BA}\}} \max_{\{D_A, D_B\}} L_G, \quad (13)$$

$$C^* = \arg \min_{\{C\}} L_C. \quad (14)$$

Since the translators  $G_{AB}, G_{BA}$  and the discriminators  $D_A, D_B$  are jointly optimized with  $C, G_{AB}$  and  $G_{BA}$  generate effective translated samples that assist improvement of classification accuracy for  $C$ .

## Experiments

**Dataset configuration** The proposed methods are evaluated with datasets, those are (1) *Face liveness* and (2) *Dogs vs. Cats* for visually similar binary classes. The datasets represent human faces and animals, and as a result have very different characteristics in terms of underlying structure and styles. The face liveness detection dataset<sup>1</sup>(Zhang et al.2012) contains very similar fake and real face images that have strong underlying structure and different style of texture. Note that no subjects are present in both training and test sets. Additionally, we evaluate on the dogs vs. cats classification dataset<sup>2</sup>, because they share part of similar style although they are belong to the different species. We explore varying the amount of training data available by training on different subsets containing 100%, 80%, 60%, and 40% of the examples of the original training set. The specific configuration is described in Table 8 and examples images of datasets are shown in Figure 9.

<sup>1</sup>[http://www.cbsr.ia.ac.cn/english/FASDB\\_Agreement/Agreement.pdf](http://www.cbsr.ia.ac.cn/english/FASDB_Agreement/Agreement.pdf)

<sup>2</sup><https://www.kaggle.com/c/dogs-vs-cats>



Figure 3: Example from face liveness and dogs vs. cats. (First row) The first column shows real face images. The second, third, and fourth column show fake face images those are corresponding to video display, printed photos, and face masks with real eyes. (Second row) The first column shows cat images, others show dog images.

Table 1: Configuration of experimental datasets and sub-sampled variants. LV\* and DC\* are reconfigured training datasets.

Face liveness	LV100	LV80	LV60	LV40	Test
Number of subjects	20	16	12	8	30
Live face	10,891	8,333	6,443	4,493	15,904
Fake face	34,165	26,557	20,188	13,511	49,862
Dogs vs. cats	DC100	DC80	DC60	DC40	Test
Dogs	12,500	10,000	7,500	5,000	6,253
Cats	12,500	10,000	7,500	5,000	6,235

**Networks model and parameters setting** We trained all the models in the experiments from scratch without pre-training and extra datasets. The mini-batches used to train the CNNs contained eight real samples, while four real samples and four translated samples were present in the mini-batches used for GTCNs and other compared models. All of the networks' parameters were optimized using the Adam optimizer. We do not vary the learning rate for the first half of epochs and linearly decay the rate to zero over the next half of epochs. The base learning rate is 0.0002 and the number of training epochs was set to 100. To prevent over-fitting, data augmentation transforms were applied such as rotation, intensity, color adjustment, and scaling variation. All of the classifiers in the experiments use the simple architecture consisting of six convolution layers, specifically:  $conv_{3 \times 3}^{16} - pool_{2 \times 2}^{max} - conv_{3 \times 3}^{16} - pool_{2 \times 2}^{max} - conv_{3 \times 3}^{32} - pool_{2 \times 2}^{max} - conv_{3 \times 3}^{32} - pool_{2 \times 2}^{max} - conv_{3 \times 3}^{64} - conv_{3 \times 3}^{64} - pool_{2 \times 2}^{avg} - do - FC_k$ , where  $do$  is dropout regularization,  $FC$  is a fully connected layer for  $k$  classes,  $pool$  is a pooling layer, and  $conv_{n \times n}^m$  consists of  $m$  convolution kernels with size  $n \times n$ , batch normalization, and rectified linear units. As the baseline translator network, we adapt the implementation of CycleGAN. Regarding the hyper parameters,  $\lambda$  was set to 10 in all experiments. The hyperparameters for the quadruplet loss were set to:  $\{\eta_a/\eta_b=2, \eta_c=6\}$  for face liveness,  $\{\eta_a/\eta_b=0.5, \eta_c=8\}$  for dogs vs. cats.

**Evaluation methods** Binary classification is the problem of deciding to which class  $y \in Y = \{A, B\}$  a given test image  $x$  belongs. Instead of using the Softmax output that was used for training, we utilize logit values obtained before

Table 2: Evaluation results of training with small volume of the face liveness dataset. ACC is mean accuracy. Cells in columns of FAR show percentage value of TAR.

Model	Dataset	ACC	FAR= $\frac{1}{100}$	FAR= $\frac{1}{1k}$	FAR= $\frac{1}{5k}$	FAR= $\frac{1}{50k}$
CNN	LV40	74.71	43.42	22.52	16.90	9.75
CNN	LV60	81.16	50.26	27.85	20.82	13.20
CNN	LV80	86.79	64.13	41.38	27.77	22.29
CNN	LV100	84.87	69.33	45.38	32.77	21.72
BC	LV40	88.62	43.13	17.78	12.61	5.28
BC <sup>+</sup>	LV40	86.09	28.10	11.78	7.65	5.48
LSGAN	LV40	79.62	60.88	37.47	30.25	23.58
VAE	LV40	90.57	67.93	42.71	32.94	17.54
Semi-sup.	LV40	89.89	58.49	41.95	33.63	21.64
GTCN	LV40	<b>92.26</b>	<b>74.81</b>	<b>62.36</b>	<b>54.04</b>	<b>39.01</b>

calculating the Softmax. Outputs of the  $FC$  layer in the classifier  $C$  are utilized to calculate a score for class  $A$  as:  $SC(y = A|x; \theta_C) = \frac{FC_A - FC_B}{2}$ , where  $FC_A$  is a logit value for class  $A$ ,  $FC_B$  is a logit value for class  $B$ ,  $SC(y = A)$  is the score for class  $A$ . The calculated  $SC(y = A)$  is employed to decide on the class as follows:

$$C(x; \theta_C) = \begin{cases} y = A & \text{if } SC(y = A) \geq th \\ y = B & \text{otherwise} \end{cases}, \quad (15)$$

where  $th$  is an acceptance threshold to decide if  $x$  is a class  $A$ . For example, if  $th$  is set to be high, then we can calculate TAR for overall test samples at low FAR.

**Training with small volume of dataset** First, we evaluate performance of baseline CNNs on different subsets of the training set to study the effect of data scarcity. In addition to this, other compared methods and the proposed GTCN are trained with only 40% of training data. We compared our method to between-class learning (BC/BC<sup>+</sup>)(Tokozume, Ushiku, and Harada2018) and semi-supervised learning with employing  $N+1$  classes (Semi-sup.)(Salimans et al.2016). In terms of generative models, we consider a least-squares GAN (LSGAN)(Mao et al.2017) and a variational autoencoder (VAE)(Kingma and Welling2013) as alternative methods to be compared. Table 2 and Table 3 show evaluation results. As the two binary classes are visually similar and lack of diverse data, baseline CNNs have low accuracy despite using deep networks and 100% of training data in both of datasets. The overall sparsity of training data causes a poor true acceptance rate. Interestingly, BC/BC<sup>+</sup> did not fare better than CNNs in the range of low false acceptance rates, although mean accuracy for those methods was however higher than for CNNs. We hypothesize this is due to the fact BC/BC<sup>+</sup> may be hard to produce good mixing data in cases where classes are very similar, caused by the proximity of the manifolds corresponding to those classes. All deep generative models outperformed the CNN baseline for LV40 dataset. In particular, VAE-based methods achieve a good accuracy, most likely because such methods generate diverse samples. For all evaluation datasets, GTCNs that were trained with 40% of the dataset clearly outperformed all of other compared methods including CNNs trained on 100% of training data.

Table 3: Evaluation results of training with small volume of the dogs vs. cats dataset. EER is the equal error rate.

Model	Dataset	ACC	FAR= $\frac{1}{100}$	FAR= $\frac{1}{1k}$	FAR= $\frac{1}{5k}$	EER
CNN	DC40	92.74	79.49	54.82	37.26	7.50
CNN	DC60	93.38	81.92	65.71	44.03	6.60
CNN	DC80	93.63	82.90	66.43	42.85	6.25
CNN	DC100	93.96	82.98	63.96	58.83	6.06
BC	DC40	92.82	77.13	28.77	5.16	7.23
BC <sup>+</sup>	DC40	92.33	69.94	23.08	4.78	8.14
LSGAN	DC40	93.13	79.44	54.88	25.07	6.84
VAE	DC40	92.89	79.10	56.97	50.97	7.12
Semi-sup.	DC40	92.67	76.26	57.64	37.21	7.18
GTCN	DC40	<b>94.28</b>	<b>84.15</b>	<b>67.41</b>	<b>54.18</b>	<b>5.66</b>

Table 4: Evaluation results of training with full volume of the face liveness dataset(LV100). All of models use images of  $128 \times 128$  pixels, except the CNN-256, which uses  $256 \times 256$ . \* are results of score fusion based model.

Single	ACC	FAR= $\frac{1}{100}$	FAR= $\frac{1}{1k}$	FAR= $\frac{1}{5k}$	FAR= $\frac{1}{50k}$
CNN	84.87	69.33	45.38	32.77	21.72
CNN-256	91.09	81.68	64.51	58.87	48.16
BC	90.17	56.93	23.84	16.53	10.92
BC <sup>+</sup>	91.19	52.97	29.28	21.20	8.51
LSGAN	93.88	81.21	50.97	37.19	26.24
VAE	95.50	86.71	77.78	70.09	61.63
Semi-sup.	94.65	76.75	43.26	31.18	18.04
GTCN	<b>97.65</b>	<b>93.62</b>	<b>86.74</b>	<b>81.81</b>	<b>76.73</b>
CNN*	95.76	93.15	82.12	79.41	61.94
CNN-256*	97.69	96.34	91.57	83.62	74.16
GTCN*	<b>99.03</b>	<b>98.87</b>	<b>95.99</b>	<b>90.73</b>	<b>85.76</b>

Table 5: Evaluation results of training with full volume of the dogs vs. cats dataset(DC100). CNN-256 uses  $256 \times 256$ .

Model	ACC	FAR= $\frac{1}{100}$	FAR= $\frac{1}{1k}$	FAR= $\frac{1}{5k}$	EER
CNN	93.96	82.98	63.96	58.83	6.06
CNN-256	95.52	89.83	78.85	69.03	4.51
BC	93.79	78.46	32.98	17.93	6.49
BC <sup>+</sup>	93.68	83.80	38.83	19.44	7.00
LSGAN	95.21	86.09	72.46	58.41	4.81
VAE	94.58	84.88	68.24	60.14	5.49
Semi-sup.	94.86	85.32	67.30	59.50	5.18
GTCN	<b>95.61</b>	<b>88.44</b>	<b>75.22</b>	<b>66.72</b>	<b>4.37</b>

**Training with the full dataset** In this experiment, we used 100% of the training dataset to verify the scalability of the proposed methods. We added CNN-256 models that are trained and tested on images of size  $256 \times 256$  pixels, while other models use images of size  $128 \times 128$  pixels. Table 4 and Table 5 show evaluation results. In a similar fashion to the experiments using reduced versions of the datasets, the performance of data augmentation methods BC/BC<sup>+</sup> and the compared deep generative models that mainly employ intra-class data augmentation show limited performance. VAEs and BC methods show relatively good performance in the face liveness dataset, since faces are highly structured images. However,

Table 6: Performance comparisons with the deep learning based face liveness detection methods

Method	EER	Image	Parameter	Methods
Yang et al.2014	4.95	128×128	58M	AlexNet+ SVM
Li et al.2016	4.50	224×224	150M	VGG19+ SVM
Atoum et al.2017	2.67	128×128	11M	CNN (10 patch+ depth)
Nguyen et al.2018	1.70	224×224	150M	VGG19+ MLBP+SVM
CNN*	3.78	128×128	0.14M	CNN (Face+ Context)
CNN-256*	2.53	256×256	0.14M	CNN (Face+ Context)
GTCN	3.49	128×128	0.07M	CNN (Face)
GTCN	2.09	128×128	0.07M	CNN (Context)
GTCN*	<b>1.02</b>	128×128	0.14M	CNN (Face+ Context)

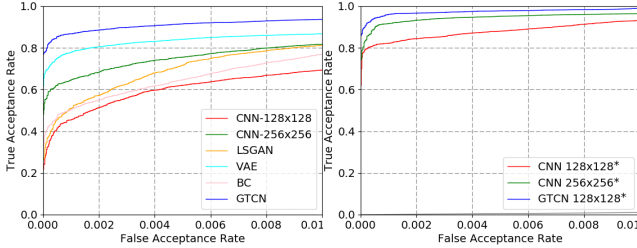


Figure 4: Receiver Operating Characteristic (ROC) comparison of models trained with full volume of the Faceliveness dataset. (Left) ROC curves of single models (Right) ROC curves of two patches based models

in both evaluation datasets, GTCNs outperform all of other compared methods including CNNs trained with a larger input, 256×256 pixels. As a matter of course, a small size of input can lead to two advantages, 1) light-weight inference and 2) recognizing far-distance images.

Lastly, to achieve a top accuracy in ranges of low false acceptance rate for the face liveness dataset, two image patches are utilized to construct score fusion based models. Those are a resized patch on a detected face region and a resized whole image that has contextual information. The proposed methods outperform previous state-of-the-art models and score fusion based models of CNN and CNN-256 as shown in table 6 without pretraining with extra datasets, large networks, and combining SVM with traditional hand craft features. Note that our two patches based model is lighter and faster than others, since we used a light-weight CNN that has just 73,904 parameters. Figure 4 shows the ROC curves for single models and two patches based models. GTCNs achieve superior true acceptance rates in the range of low false acceptance rates.

## Discussion

**Ablation Study** We perform an ablation study, the results of which are shown in Table 10. As first, we trained  $G_{AB}$  and  $G_{BA}$  separately and used translators with fixed parameters to augment data for training  $C$ . *Separate* learning shows better accuracy than baseline CNN, because translators generate diverse data. However, proposed *Joint* learning is superior to *Separate* learning. One of the disadvantages of *Separate* learning is that it takes longer to train, since two models are trained sequentially. To analyze the effect of each component

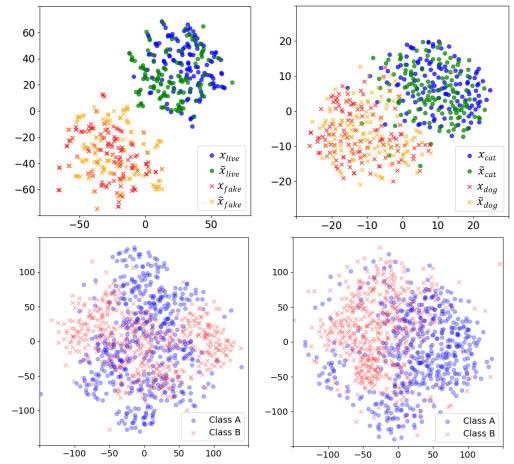


Figure 5: First two plots show examples of t-SNE analysis for training data on GTCN: (1) Face liveness and (2) Dogs vs. cats. The augmented data points  $\tilde{x}$  achieve a good coverage of all the area of the embedding space corresponding to their true class in binary classification. We can consider that they are good at augmenting training data in that regard. Second two plots show comparison of methods by t-SNE analysis for LV40 test dataset: (3) CNN and (4) the proposed GTCN

of the GTCN, learning options were adapted sequentially. AF stands for adaptive fade-in learning, QL for quadruplet loss, and ST corresponds to stochastic translation. Because translated images could be sometimes suppressed by applying AF during joint training, the performance are not much improved on binary classification. However, when AF, QL and ST are applied simultaneously, the performance of GTCNs is fairly improved, since ST contributes data diversity, QL increases fisher’s criterion, and AF controls noisy images.

**Visualization of train and test features** We provide the results of a t-distributed stochastic neighbor embedding (t-SNE Maaten and Hinton2008) visualization in Figure 5. Since GTCNs produce translated data from given real data, the feature space of augmented training samples are visualized. Additionally, the feature space of the classifiers for test samples of the face liveness dataset is visualized. The t-SNE of the GTCN with our proposed methods results in a sharper distinction between examples of similar classes, highlighting the fact that the learned representation is of higher quality.

Table 7: Ablation experimental results of the proposed methods on the datasets

	Face liveness	CNN	Separate	+Joint	+AF	+AF/QL	+AF/QL/ST
Accuracy	84.87	94.93	96.43	95.35	97.04	<b>97.65</b>	
FAR= $\frac{1}{50k}$	21.72	27.15	67.10	55.71	74.42	<b>76.73</b>	
	Dogs vs. cats	CNN	Separate	+Joint	+AF	+AF/QL	+AF/QL/ST
Accuracy	93.96	95.05	95.44	95.72	94.93	<b>95.61</b>	
FAR= $\frac{1}{5k}$	58.83	42.25	64.38	57.37	60.29	<b>66.72</b>	

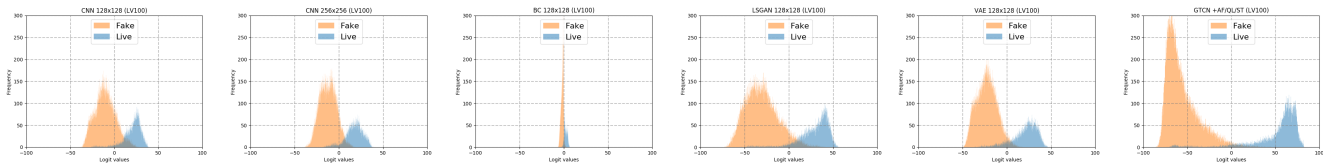


Figure 6: Histograms of logit values for liveness test dataset. The compared models are trained on LV100 dataset. (1) CNN  $128 \times 128$  (2) CNN  $256 \times 256$  (3) BC  $128 \times 128$  (4) LSGAN  $128 \times 128$  (5) VAE  $128 \times 128$  (6) GTCN  $128 \times 128$

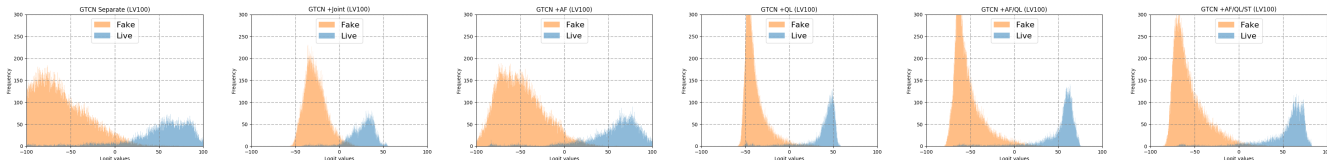


Figure 7: Histograms of logit values for liveness test dataset. The compared models are trained on LV100 dataset. (1) GTCN Separate (2) GTCN +Joint (3) GTCN +AF (4) GTCN +QL (5) GTCN +AF/QL (6) GTCN +AF/QL/ST

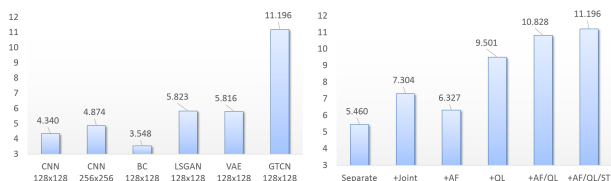


Figure 8: Comparison of Fisher's criterion scores. Vertical axis on the charts represents score  $J$ . (Up) Compared methods (Down) Ablation study results of the proposed GTCN

**Characteristics for within and between classes** Fisher's criterion (Fisher1936) score is used to analyze the classifiers. Fisher's score  $J$  in the experiment is defined as:

$$J = \frac{|\mu_A - \mu_B|^2}{\sigma_A^2 + \sigma_B^2}, \quad (16)$$

where  $\mu_A$  and  $\mu_B$  are the mean of the logits for distribution A and B respectively.  $\sigma_A$  and  $\sigma_B$  denote the standard deviations of the same logits. The comparison of Fisher's criterion scores for face liveness detection are shown in Figure 8. The proposed GTCN shows the best score, while other generative models show better scores than baseline CNNs. However, BC achieves lower score than the CNNs. In the ablation study results, utilizing all the proposed methods, Joint/AF/QL/ST, results in the best score. To clarify understanding for the scores, the histogram analysis of logit values for liveness test dataset are shown in Figure 6 and Figure 7. CNN $256 \times 256$  seems to outperform CNN $128 \times 128$ . In case of BC, intra-class variance and mean difference between classes are both reduced. In VAE and GAN, intra-class variance and inter-class margin are both increased. The proposed GTCN enlarges margin well between live class and fake class. In the ablation study, Joint, AF, QL, and ST show different characteristics to form the class distribution. Joint learning makes smaller variance within each class than Separate learning, while AF enlarges margin between classes. QL apparently reduces variance of each class, while it enlarges margin between the classes.



Figure 9: Example from artist datasets. The first column shows Van Gogh's painting. The second, third, and fourth column show Monet, Cezanne, and Ukiyoe's one.

Table 8: Configuration of experimental datasets and subsampled variants. AT\* are reconfigured training datasets.

Artist	AT100	AT80	AT60	AT40	Test
Cezanne	291	231	173	115	292
Monet	597	477	358	238	586
Ukiyoe	412	329	247	164	413
Van Gogh	200	160	120	80	200

## More experiments and analysis

### Multi-class style classification

We extend the proposed method to a multi-class style classification setting. As an example of the cases with lack of data, artists usually draw a limited number of paintings in their lifetime, which makes artist classification a challenging problem. We constructed the artist dataset<sup>3</sup> that contains paintings from four painters as a multi-class classification experiment. Paintings have little overall structure, despite the styles chosen being similar, which creates a challenging problem of artist classification.

This requires a slight modification of our proposed approach.  $G_{AB}(\cdot)$  and  $G_{BA}(\cdot)$  are trained as two translators across multiple-classes. A mini-batch size is set to four and we sample examples from the mini-batch belonging to different classes. Specifically, we use the same architecture as the one in the main paper, which has only two generators,

<sup>3</sup><https://github.com/GTCN/datasets>

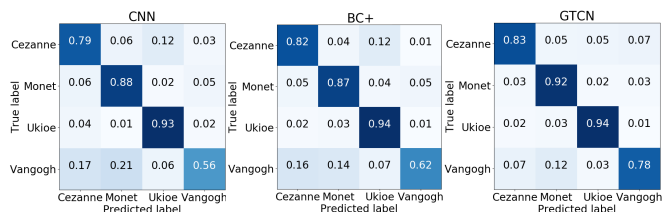


Figure 10: Comparison of confusion matrix for compared methods on the artist dataset

Table 9: Comparison of mean accuracy on multi-class artist dataset

Model	AT100	AT80	AT60	AT40
CNN	83.21	80.95	77.68	69.42
CNN-256	87.28	86.54	83.21	72.42
BC	83.08	82.41	78.95	69.62
BC <sup>+</sup>	84.74	82.74	79.55	68.95
Semi-sup.	86.81	84.68	80.55	71.75
GTCN	<b>88.81</b>	<b>86.81</b>	<b>81.55</b>	<b>75.62</b>

Table 10: Ablation experimental results of the proposed methods on the datasets

Artist	CNN	Separate	+Joint	+AF	+AF/QL	+AF/QL/ST
Accuracy	83.21	82.61	85.14	85.88	86.21	<b>88.81</b>

via a simple trick of setting minibatch size to be four consisting of only one  $x_A$ , one  $\tilde{x}_A$ , one  $x_B$ , and one  $\tilde{x}_B$  meaning that each minibatch handles only two classes at a time. To calculate the probability for multi-class  $k$  from a given test image  $x$ , we employ the softmax output of the network. The function is defined by  $P(y = i|x; \theta_C) = \frac{\exp(FC_i)}{\sum_{j=1}^k \exp(FC_j)}$ , where  $1 \leq i \leq k$  is a class-id,  $x$  is a given image, and  $k$  is the number of classes. We choose the class-id with the maximum probability among  $k$  probabilities as the recognized class-id of  $x$ .

Evaluation results are shown in Table 9 and GTCNs outperform compared methods. The accuracy for the four classes improved evenly for the GTCN as shown in Figure 10, because translated samples were used for training. We perform an ablation study, the results of which are shown in Table 10. Note that this is more like a simple modification for multi-class classification rather than carefully designed extension. However, it is noteworthy that because of joint training of GAN and classifier, the proposed method achieves 88.81% of accuracy for artist dataset significantly outperforming the baseline CNN (83.21%) or separate training of GAN and CNN (82.61%). In terms of characteristics for within and between classes, 2D PCA of logit values for artist test dataset are shown in Figure 15 and Figure 16, to analyze multi-class classification results. Characteristics of comparison with other methods and ablation study are very similar to binary classification cases. Overall results show the proposed GTCN enlarges margin between classes and reduce variance of within class.

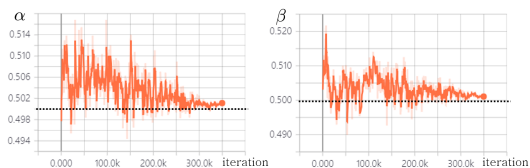


Figure 11: Example variation of  $\alpha$  and  $\beta$  for adaptive fade-in learning

**Effects of fine-tuning for multi-class task** After training GTCNs, we additionally fine-tune the classifier with a cross-entropy loss for a few epochs. The method quickly stabilizes and improves the overall accuracy of the classifier in GTCNs for a multi-class problem. By fine-tuning, we assume weights related to noisy samples of multi-class may be truncated. To perform a fair comparison, we tried applying fine-tuning to other compared methods such as CNNs and BC/BC<sup>+</sup>s. The fine-tuning is only useful for GTCN. To illustrate this, we report results of fine-tuning the other methods. There was no meaningful improvement and performance was sometimes degraded as shown in Table 11.

Table 11: Comparison for effects of fine-tuning on the artist dataset. †denotes fine-tuning is applied.

Model	AT100	AT80	AT60	AT40
BC	<b>83.48</b>	<b>81.61</b>	<b>78.81</b>	<b>71.22</b>
†BC	81.88	80.28	77.28	70.15
BC <sup>+</sup>	<b>84.74</b>	<b>82.74</b>	<b>79.55</b>	68.95
†BC <sup>+</sup>	83.48	79.75	77.75	<b>70.02</b>
GTCN	85.01	80.81	76.48	70.75
†GTCN	<b>88.81</b>	<b>86.81</b>	<b>81.55</b>	<b>75.62</b>

### Hyper-parameters search for quadruplet loss

The proposed quadruplet loss uses hyper-parameters such as  $\eta_a$ ,  $\eta_b$ , and  $\eta_c$  in the main paper. To achieve the best performance, we perform a grid-search of hyper-parameters on the dogs vs. cats and artist dataset as shown in Table 12 and 13. The hyperparameters for the quadruplet loss were set to:  $\{\eta_a/\eta_b=0.25, \eta_c=1.5\}$  for the artist dataset. The hyper-parameters for the quadruplet loss have an impact on accuracy.

### Parameter movements of adaptive fade-in

Figure 11 shows the values taken by  $\alpha$  and  $\beta$  for the AF method during training of the face liveness dataset. At the start of training,  $\alpha$  and  $\beta$  were higher than 0.5, because real images are more confidently classified than generated images, while the values have almost converged to 0.5 at the end of training in the example.

### Visual examples of trained images

The GTCN uses progressively translated images as a part of the mini-batches. Note that the main purpose of the GTCN is not to generate realistic images but rather to improve the



Table 12: Examples of hyper-parameters obtained by grid search on the dogs vs. cats dataset.

$\eta_a / \eta_b$	$\eta_c$	ACC	$FAR=\frac{1}{100}$	$FAR=\frac{1}{1k}$	$FAR=\frac{1}{5k}$	EER
<b>0.5</b>	<b>8</b>	<b>95.61</b>	<b>88.44</b>	75.22	<b>66.72</b>	<b>4.37</b>
0.5	4	95.16	86.22	71.71	56.94	4.86
0.5	2	95.12	85.82	71.34	57.55	5.01
0.25	4	94.95	84.91	66.61	60.27	5.09
0.25	2	95.49	87.55	65.60	60.95	4.45
0.25	1	95.44	88.40	<b>76.02</b>	58.73	4.51

Table 13: Examples of hyper-parameters obtained by grid search on the artist dataset.

$\eta_a / \eta_b$	$\eta_c$	ACC
0.5	2.5	85.94
0.5	2.0	86.41
<b>0.25</b>	<b>1.5</b>	<b>88.81</b>
0.25	1.0	86.08

classifier’s accuracy. Nonetheless, a visual inspection of translated/generated samples gives insights into why certain methods work better than others.

As shown in Figure 12, all of the compared models generate visually different images from given inputs to construct the augmented mini-batch. The images generated by the VAE are blurry and seem to wrongly interpolate across classes. BC attempts to mix up images, but seems to go pear-shaped at generating images that realistically belong to the target class, especially for the images of the artist dataset that display less overall structure. However, the GTCN attempts to borrow structure and shape information from samples of different classes while usually preserve texture and style, so the classifier can learn with sharper and more diverse training data. To show more examples of augmented training images, visually informative pairs were chosen in Figure 14.

## Miscellaneous design of GTCN

### Light-weight classifier $C$

We chose to adopt an architecture that is sufficiently light-weight so as to run on performance-critical systems such as smartphones. The light-weight model is a CNN consisting of 6 convolutional layers (in addition to pooling and fully-connected components). The parameters are denoted:

$$\theta_C = \{w^1, w^2, w^3, w^4, w^5, w^6, w^s\}. \quad (17)$$

The specific parameters for the network are given in Table 14. As  $\theta_C$  only consists of 73,904 ( $k=2$ ) / 75,952 ( $k=4$ ) parameters, the trained networks  $C$ s have a small memory footprint and can be run on smart devices in real-time without GPU acceleration.

### Score fusion models

As we described in the main paper, we use score fusion models to achieve the best accuracy in face liveness detection. In detail, two kinds of image patches are used in each classifier  $C$  in the GTCNs. Example of patches are shown in Figure 13. For the face liveness detection experiments, we employed a face detector (Viola and Jones2001) and resized the detected



Figure 12: Qualitative comparison of data augmentation methods to train a classifier. First two rows are binary class examples of the face liveness and the dogs vs. cats dataset. Last three rows are multi-class examples of the artist dataset. In the examples, BC uses 0.33 and 0.66 as mixing ratio between two images.



Figure 13: Examples of image patches: resized detected face  $x_{rs}$ , and resized contextual  $x_{ct}$  from input image  $I$ . Note that  $x_{rs}$  and  $x_{ct}$  are images of  $128 \times 128$  pixels.

regions to obtain normalized images that have RGB channels with  $128 \times 128$  pixels. The ensemble of  $C$  tries to capture the difference of global shapes, reflection pattern, local texture, and contextual information from a single color image.

Formally, we consider two classifiers,  $C_{rs}$  and  $C_{ct}$ . The classifier  $C_{rs}$  that discern texture and reflection pattern is given by

$$SC_{rs} = C_{rs}(x_{rs}; \theta_{rs}), \forall x_{rs} \in Resize(FD(I)), \quad (18)$$

where  $SC_{rs}$  is a liveness score of a patch  $x_{rs}$  that is a resized

Table 14: Design of a light-weight classifier  $C$ . Resolution of input image  $x$  is  $128 \times 128$ .  $Conv$  stands for a convolutional layer,  $BN$  for batch normalization,  $ReLU$  for rectified linear units, and  $Pool$  corresponds to a pooling layer.  $FC$  denotes a fully connected layer.  $k$  is the number of classes for  $y \in Y$ .

Layers	Parameters	Outputs
$Conv1-BN-ReLU$ $Pool1$	$w^1: 3 \times 3 \times 3$ , kernels=16 max: $2 \times 2$ , stride=2	$128 \times 128 \times 16$ $64 \times 64 \times 16$
$Conv2-BN-ReLU$ $Pool2$	$w^2: 3 \times 3 \times 16$ , kernels=16 max: $2 \times 2$ , stride=2	$64 \times 64 \times 16$ $32 \times 32 \times 16$
$Conv3-BN-ReLU$ $Pool3$	$w^3: 3 \times 3 \times 16$ , kernels=32 max: $2 \times 2$ , stride=2	$32 \times 32 \times 32$ $16 \times 16 \times 32$
$Conv4-BN-ReLU$ $Pool4$	$w^4: 3 \times 3 \times 32$ , kernels=32 max: $2 \times 2$ , stride=2	$16 \times 16 \times 32$ $8 \times 8 \times 32$
$Conv5-BN-ReLU$ $Conv6-BN-ReLU$	$w^5: 3 \times 3 \times 32$ , kernels=64 $w^6: 3 \times 3 \times 64$ , kernels=64	$8 \times 8 \times 64$ $8 \times 8 \times 64$
$Pool6$ $Dropout$	average: $2 \times 2$ , stride=2 -	$4 \times 4 \times 64$ 1024
$FC$ $Softmax$	$w^s: 1024 \times k$ -	$k$ $P(y x)$

image of a detected face region,  $FD$  is a face detector, and  $\theta_{rs}$  are learned parameters. Similarly, the classifier  $C_{ct}$  that discriminates global shapes and contextual pattern is given by

$$SC_{ct} = C_{ct}(x_{ct}; \theta_{ct}), \forall x_{ct} \in Resize(I), \quad (19)$$

where  $SC_{ct}$  is a liveness score of a patch  $x_{ct}$  that is a resized contextual image from an input image  $I$ , and  $\theta_{ct}$  are learned parameters. To decide whether the given image  $I$  is live or not, the final liveness score is calculated by

$$SC = \alpha_{rs} \times SC_{rs} + \alpha_{ct} \times SC_{ct}, \quad (20)$$

where  $\alpha_{rs}$  and  $\alpha_{ct}$  are coefficient values to combine scores from two models to perform liveness prediction with a late fusion method. In this paper, we set  $\alpha_{rs}=1$  and  $\alpha_{ct}=0.6$ , respectively.

## Conclusion

We propose novel joint learning methods on GTCN that train a generative translation model and a classifier via augmented mini-batch technique, adaptive fade-in learning, and quadruplet loss. Since translators provide challenging data incrementally during training a classifier, accuracy can be improved by employing the augmented inter-class data. After the end of training, we perform inference using only the light-weight classifier of GTCN. Our method trained on a small subset of the whole dataset achieves a greater accuracy than the baselines trained on the full dataset. When training on the full dataset, we surpass comparable state-of-the-art methods despite using low resolution images and a smaller network architecture for our method. We believe our work can benefit classification tasks that suffer from visual similarity, diversity, and lack of data.

## References

- [2017] Akbulut, Y.; Şengür, A.; Budak, Ü.; and Ekici, S. 2017. Deep learning based face liveness detection in videos. In *Artificial Intelligence and Data Processing Symposium (IDAP), 2017 International*, 1–4. IEEE.
- [2018] Almahairi, A.; Rajeswar, S.; Sordoni, A.; Bachman, P.; and Courville, A. 2018. Augmented cyclegan: Learning many-to-many mappings from unpaired data. *arXiv preprint arXiv:1802.10151*.
- [2017] Antoniou, A.; Storkey, A.; and Edwards, H. 2017. Data augmentation generative adversarial networks. *arXiv preprint arXiv:1711.04340*.
- [2017] Atoum, Y.; Liu, Y.; Jourabloo, A.; and Liu, X. 2017. Face anti-spoofing using patch and depth-based cnns. In *Biometrics (IJCB), 2017 IEEE International Joint Conference on*, 319–328. IEEE.
- [2016] Chen, X.; Duan, Y.; Houthoofd, R.; Schulman, J.; Sutskever, I.; and Abbeel, P. 2016. Infogan: Interpretable representation learning by information maximizing generative adversarial nets. In *Advances in Neural Information Processing Systems*, 2172–2180.
- [2017] Chen, W.; Chen, X.; Zhang, J.; and Huang, K. 2017. Beyond triplet loss: a deep quadruplet network for person re-identification. In *The IEEE Conference on Computer Vision and Pattern Recognition (CVPR)*, volume 2.
- [2017] Choi, Y.; Choi, M.; Kim, M.; Ha, J.-W.; Kim, S.; and Choo, J. 2017. Stargan: Unified generative adversarial networks for multi-domain image-to-image translation. *arXiv preprint arXiv:1711.09020*.
- [2017] Chongxuan, L.; Xu, T.; Zhu, J.; and Zhang, B. 2017. Triple generative adversarial nets. In *Advances in Neural Information Processing Systems*, 4091–4101.
- [2018] Creswell, A.; White, T.; Dumoulin, V.; Arulkumaran, K.; Sengupta, B.; and Bharath, A. A. 2018. Generative adversarial networks: An overview. *IEEE Signal Processing Magazine* 35(1):53–65.
- [2017] Dai, Z.; Yang, Z.; Yang, F.; Cohen, W. W.; and Salakhutdinov, R. R. 2017. Good semi-supervised learning that requires a bad gan. In *Advances in Neural Information Processing Systems*, 6513–6523.
- [2016] Dumoulin, V.; Belghazi, I.; Poole, B.; Mastropietro, O.; Lamb, A.; Arjovsky, M.; and Courville, A. 2016. Adversarially learned inference. *arXiv preprint arXiv:1606.00704*.
- [1936] Fisher, R. A. 1936. The use of multiple measurements in taxonomic problems. *Annals of eugenics* 7(2):179–188.
- [2017] Gan, Z.; Chen, L.; Wang, W.; Pu, Y.; Zhang, Y.; Liu, H.; Li, C.; and Carin, L. 2017. Triangle generative adversarial networks. In *Advances in Neural Information Processing Systems*, 5253–5262.
- [2014] Goodfellow, I.; Pouget-Abadie, J.; Mirza, M.; Xu, B.; Warde-Farley, D.; Ozair, S.; Courville, A.; and Bengio, Y. 2014. Generative adversarial nets. In *Advances in neural information processing systems*, 2672–2680.
- [2018] Huang, X.; Liu, M.-Y.; Belongie, S.; and Kautz, J. 2018. Multimodal unsupervised image-to-image translation. *arXiv preprint arXiv:1804.04732*.

- [2017] Isola, P.; Zhu, J.-Y.; Zhou, T.; and Efros, A. A. 2017. Image-to-image translation with conditional adversarial networks. *arXiv preprint*.
- [2013] Kingma, D. P., and Welling, M. 2013. Auto-encoding variational bayes. *arXiv preprint arXiv:1312.6114*.
- [2018] Lee, H.-Y.; ; Tseng, H.-Y.; Huang, J.-B.; Singh, M. K.; and Yang, M.-H. 2018. Diverse image-to-image translation via disentangled representations. In *European Conference on Computer Vision*.
- [2018] Li, H.; He, P.; Wang, S.; Rocha, A.; Jiang, X.; and Kot, A. C. 2018. Learning generalized deep feature representation for face anti-spoofing. *IEEE Transactions on Information Forensics and Security* 13(10):2639–2652.
- [2017] Liu, M.-Y.; Breuel, T.; and Kautz, J. 2017. Unsupervised image-to-image translation networks. In *Advances in Neural Information Processing Systems*, 700–708.
- [2018] Liu, Y.; Jourabloo, A.; and Liu, X. 2018. Learning deep models for face anti-spoofing: Binary or auxiliary supervision. In *Proceedings of the IEEE Conference on Computer Vision and Pattern Recognition*, 389–398.
- [2008] Maaten, L. v. d., and Hinton, G. 2008. Visualizing data using t-sne. *Journal of Machine Learning Research* 9(Nov):2579–2605.
- [2017] Mao, X.; Li, Q.; Xie, H.; Lau, R. Y.; Wang, Z.; and Smolley, S. P. 2017. Least squares generative adversarial networks. In *Computer Vision (ICCV), 2017 IEEE International Conference on*, 2813–2821. IEEE.
- [2014] Mirza, M., and Osindero, S. 2014. Conditional generative adversarial nets. *arXiv preprint arXiv:1411.1784*.
- [2016] Odena, A.; Olah, C.; and Shlens, J. 2016. Conditional image synthesis with auxiliary classifier gans. *arXiv preprint arXiv:1610.09585*.
- [2016] Odena, A. 2016. Semi-supervised learning with generative adversarial networks. *arXiv preprint arXiv:1606.01583*.
- [2013] Preston, A. R., and Eichenbaum, H. 2013. Interplay of hippocampus and prefrontal cortex in memory. *Current Biology* 23(17):R764–R773.
- [2016] Salimans, T.; Goodfellow, I.; Zaremba, W.; Cheung, V.; Radford, A.; and Chen, X. 2016. Improved techniques for training gans. In *Advances in Neural Information Processing Systems*, 2234–2242.
- [2015] Schroff, F.; Kalenichenko, D.; and Philbin, J. 2015. Facenet: A unified embedding for face recognition and clustering. In *Proceedings of the IEEE conference on computer vision and pattern recognition*, 815–823.
- [2018] Song, X.; Zhao, X.; and Lin, T. 2018. Face spoofing detection by fusing binocular depth and spatial pyramid coding micro-texture features. *arXiv preprint arXiv:1803.04722*.
- [2015] Springenberg, J. T. 2015. Unsupervised and semi-supervised learning with categorical generative adversarial networks. *arXiv preprint arXiv:1511.06390*.
- [2016] Taigman, Y.; Polyak, A.; and Wolf, L. 2016. Unsupervised cross-domain image generation. *arXiv preprint arXiv:1611.02200*.
- [2018] Tang, D.; Zhou, Z.; Zhang, Y.; and Zhang, K. 2018. Face flashing: a secure liveness detection protocol based on light reflections. *arXiv preprint arXiv:1801.01949*.
- [2018] Tokozume, Y.; Ushiku, Y.; and Harada, T. 2018. Between-class learning for image classification. In *The IEEE Conference on Computer Vision and Pattern Recognition (CVPR)*.
- [2001] Viola, P., and Jones, M. 2001. Rapid object detection using a boosted cascade of simple features. In *Computer Vision and Pattern Recognition, 2001. CVPR 2001. Proceedings of the 2001 IEEE Computer Society Conference on*, volume 1, I–I. IEEE.
- [2012] Zhang, Z.; Yan, J.; Liu, S.; Lei, Z.; Yi, D.; and Li, S. Z. 2012. A face antispoofing database with diverse attacks. In *Biometrics (ICB), 2012 5th IAPR international conference on*, 26–31. IEEE.
- [2017a] Zhu, J.-Y.; Park, T.; Isola, P.; and Efros, A. A. 2017a. Unpaired image-to-image translation using cycle-consistent adversarial networks. In *Proceedings of the IEEE Conference on Computer Vision and Pattern Recognition*, 2223–2232.
- [2017b] Zhu, J.-Y.; Zhang, R.; Pathak, D.; Darrell, T.; Efros, A. A.; Wang, O.; and Shechtman, E. 2017b. Toward multi-modal image-to-image translation. In *Advances in Neural Information Processing Systems*, 465–476.

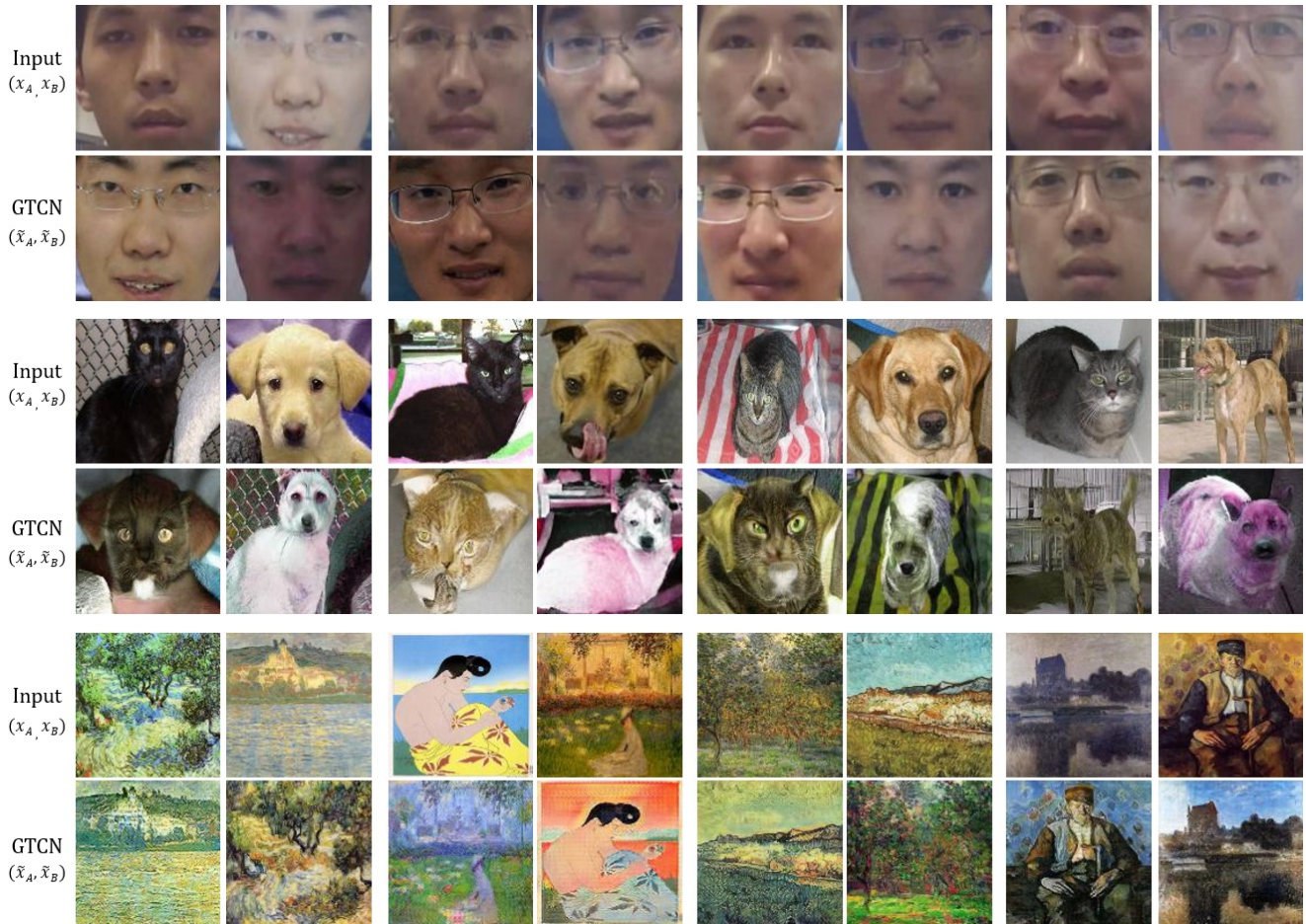


Figure 14: Examples of augmented training images for GTCN: (Up) Face liveness dataset (Middle) Dogs vs. cats dataset (Bottom) Artist dataset In the examples, translated samples attempt to borrow structure and shape information from samples of different classes while usually preserving texture and style. Even though the translated images are sometimes visually weird, the images in the inter-class space also contribute to improving of the classifier’s accuracy for visually similar images in terms of shape and style.

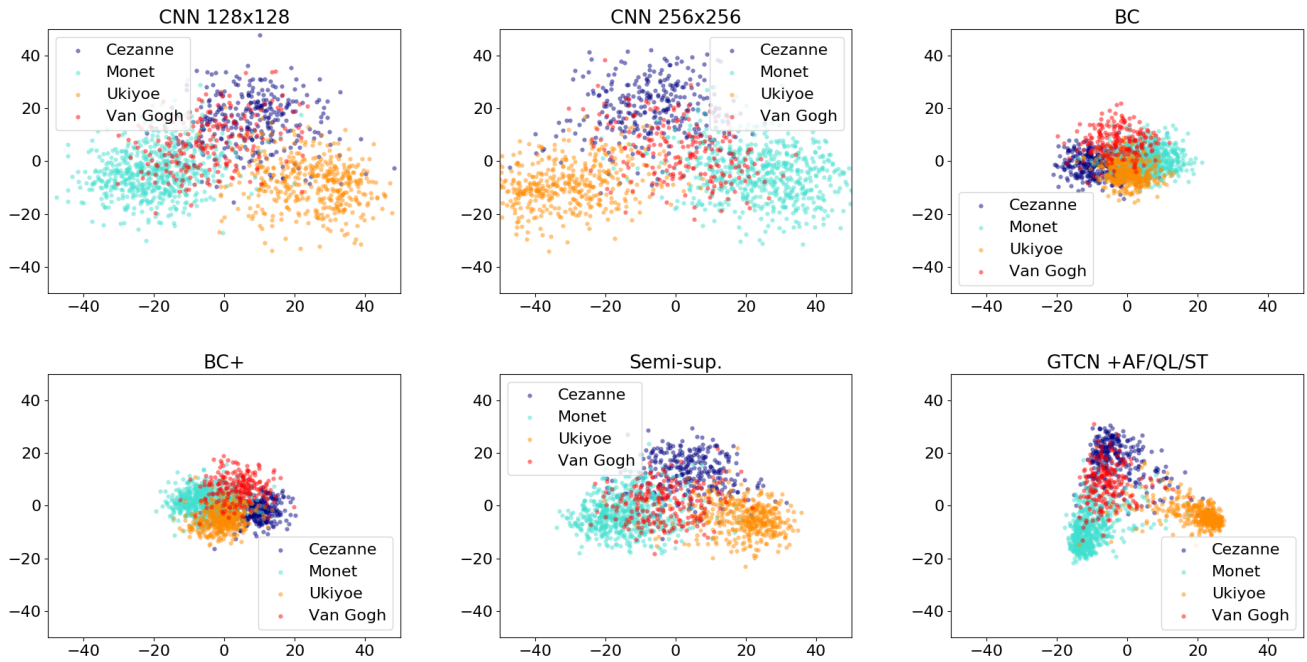


Figure 15: PCA analysis for artist test dataset. The compared models are trained on AT100 dataset. (1) CNN  $128 \times 128$  (2) CNN  $256 \times 256$  (3) BC  $128 \times 128$  (4) BC+  $128 \times 128$  (5) Semi-sup.  $128 \times 128$  (6) GTCN  $128 \times 128$

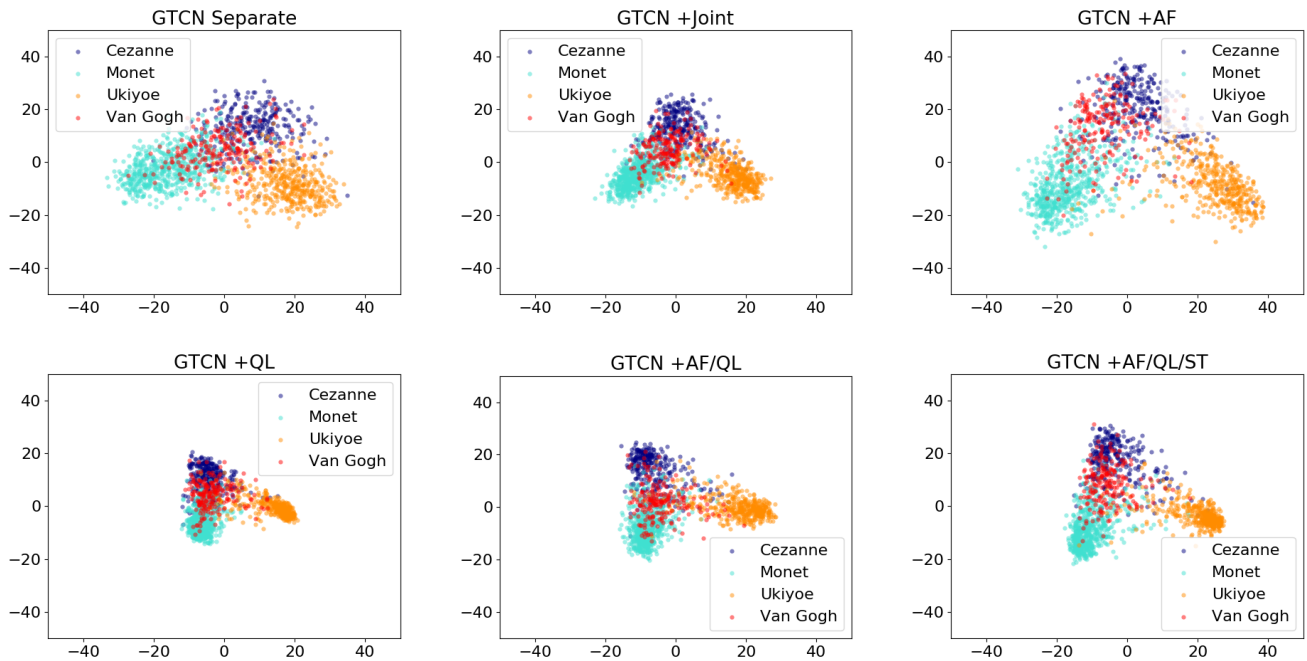


Figure 16: PCA analysis for artist test dataset. The compared models are trained on AT100 dataset. (1) GTCN Separate (2) GTCN +Joint (3) GTCN +AF (4) GTCN +QL (5) GTCN +AF/QL (6) GTCN +AF/QL/ST